JOURNAL OF MATERIALS SCIENCE 21 (1986) 2744–2752

Stress distribution in a segmented coating film on metal fibre under tensile loading

SHOJIRO OCHIAI, KOZO OSAMURA
Department of Metallurgy, Kyoto University, Kyoto 606, Japan

When a coating film on a metal fibre or wire is brittle, it exhibits multiple-fracture under loading. In order to describe the exerted tensile stress on the segments of a coating film as a function of the distance from the end of the segments and as a function of applied stress, a new approximate calculation method is presented, assuming that the interfacial bonding strength is high enough and no interfacial debonding occurs. Using the present calculation method, effects of geometrical factors such as fibre diameter, thickness of coating film and length of segment as well as those of mechanical factors such as Young's modulus, shear modulus and the yield stress of the fibre and the coating film on the exerted tensile stress on the segments and also on the exerted shear stress at the interface are described in a quantitative manner.

1. Introduction

Currently, in wide fields in technology, coating treatment on metals is carried out in order to strengthen the surface of metals or to protect them from corrosion. The materials for coating are, in general, harder than the base metals and the strain to failure is lower than the metals. Thus, in many cases, the coating film on metals fails in early stages of deformation under tensile loading, forming a notch on the metal surface. If base metals have low ductility, the notch formed can extend into the metal, resulting in a loss in strength of metals [1–3]. On the other hand, if base metals have a high enough ductility to prevent the formed notch from extending into metals, the coating film exhibits multiple-fracture as long as the drop in load due to fracture of coating film can be compensated for by work-hardening of the metals. The multiple fracture phenomenon of coating film on metals under tensile loading have been observed in aluminium–alumina [4, 5], niobium–superconducting Nb_3Sn [6, 7] and molybdenum–TiC [8, 9] combinations where the former are metals and the latter are coating materials. It is very important to describe the multiple-fracture phenomenon in these practically useful materials.

In order to describe the multiple-fracture phenomenon of coating film in a quantitative manner, we should know exerted stress in a segmented coating layer. Considering the case where a metal fibre deforms plastically in shear in the whole range of the length of segments, the exerted tensile stress on segments, σ_2, could be inferred by modifying the Kelly–Tyson model [10], by

$$\sigma_2\pi[(d + 2c)^2 - d^2]/4 = \pi d\tau x \qquad (1)$$

where d is the diameter of the fibre, c the thickness of the coating film and x the distance from the end of segments, and τ is the interfacial shear stress, which can be given by the shear yield stress of the metal if the metal shows no strain hardening. However, practical metals and alloys show more or less strain hardening, which makes it difficult to estimate the value of τ in Equation 1. Furthermore, the multiple-fracture phenomenon of the coating film occurs even at low stress levels where the fibre deforms elastically in shear along the length of the segments and also where the fibre deforms plastically in shear in some range of the length of segments but it deforms elastically in other range of the length. In order to know the tensile stress distribution and shear stress distribution at interface in the whole range of applied stress, a new approach is requested.

The aim of the present paper is to present a new approach for the case where interfacial bonding is strong enough to supress debonding at the interface. In a subsequent paper [11], using the present approach, a computer simulation is carried out and the multiple-fracture behaviour of the coating film is described in a quantitative manner.

2. Calculation method

In the present approach, the following approximation are made: (i) the fibre shows linear strain hardening after tensile and shear yielding; (ii) tensile and shear behaviour of the fibre are independent of each other; namely tensile (shear) behaviour is not affected by shear (tensile) behaviour; (iii) the radial and hoop stresses are neglected and only the tensile and shear stresses in the tensile direction are considered.

2.1. Simplification of the stress–strain curve of the fibre

In the present calculation, the tensile stress σ_1–strain ε curve of the fibre was approximated as shown in Fig. 1a. In the stage of elastic deformation ($\varepsilon < \varepsilon_y$ where ε_y is the yield strain in tension), σ_1 is given by using the

0022–2461/86 $03.00 + .12

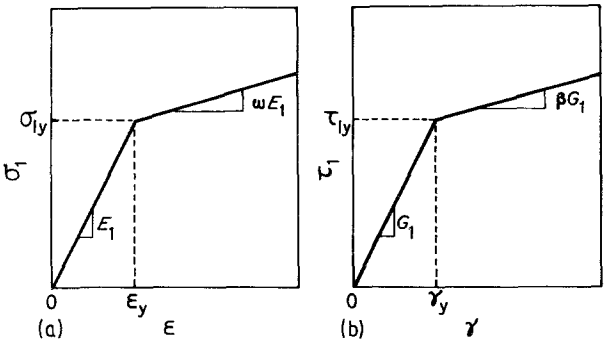

Figure 1 Simplified (a) tensile stress σ_1–strain ε and (b) shear stress τ_1–strain γ curves of the fibre.

Young's modulus E_1 as

$$\sigma_1 = E_1\varepsilon \tag{2}$$

and in the stage of plastic deformation ($\varepsilon > \varepsilon_y$), it is given by

$$\sigma_1 = (1 - \omega)\sigma_{1y} + \omega E_1\varepsilon \tag{3}$$

where σ_{1y} is the tensile yield stress given by $E_1\varepsilon_y$ and ω is the slope of the stress–strain curve in plastic deformation, normalized with respect to E_1. "$\omega = 0$", "$0 < \omega < 1$" and "$\omega = 1$" mean that the fibre exhibits no strain hardening after yielding, it deforms with the strain hardening coefficient ωE_1 and it deforms elastically, respectively.

Similarly, as shown in Fig. 1b, the shear stress τ_1–shear strain γ curve was approximated as

$$\tau_1 = G_1\gamma \tag{4}$$

for $\gamma < \gamma_y$ where γ_y is the shear yield strain and G_1 is the shear modulus, and

$$\tau_1 = (1 - \beta)\tau_{1y} + G_1\gamma \tag{5}$$

for $\gamma > \gamma_y$ where τ_{1y} is the shear yield stress of the fibre and β is the slope of the shear stress–strain curve in plastic deformation, normalized with respect to G_1.

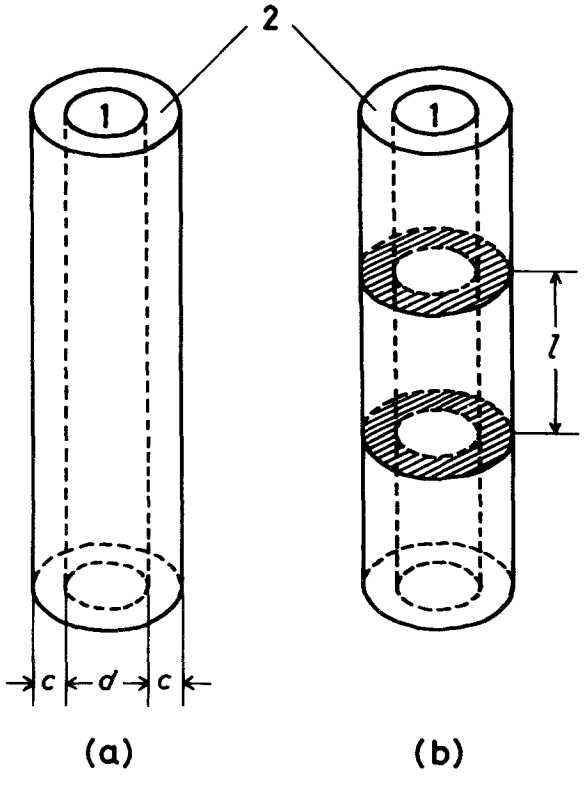

Figure 2 (a) Model composite cylinder and (b) appearance of the composite after mutliple-fracture of the coating film. The hatched region shows the cross-section of fractured coating film. 1 and 2 refer to fibre and coating film, respectively.

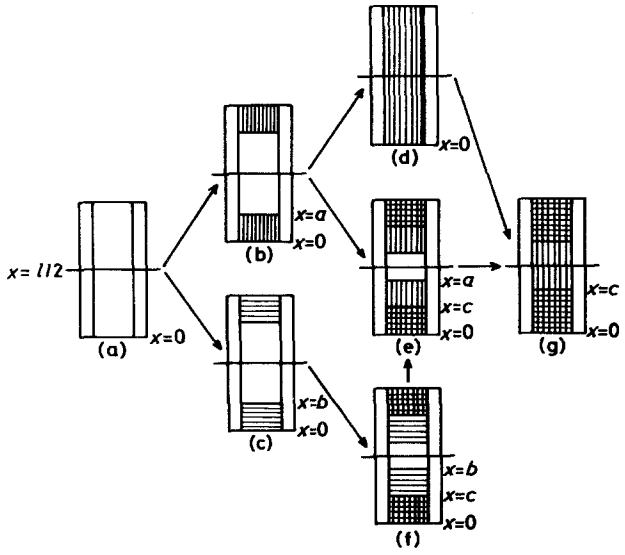

Figure 3 Deformation stages of the element with length l. □, ▨, ▤ and ▩ refer to regions A, B, C and D, respectively.

2.2. Model composite

Fig. 2a shows the two-component composite cylinder of an inner core of fibre (shown by 1) and outer case of coated layer (2). The diameter of the fibre and the thickness of the coating film are given by d and c, respectively. In the following parts, the subscripts 1 and 2 refer to the fibre and coating film, respectively.

With increasing applied load, the coating film shows multiple fracture as schematically shown in Fig. 2b. In the present calculation, the element with length l is taken and stress distribution will be calculated for this element.

2.3. Deformation stages

When the applied load is low, the fibre deforms elastically both in tension and shear (Fig. 3a). With increasing stress, the fibre becomes plastic in (b) tension or (c) in shear. With further increasing load, the range of plastic deformation of the fibre in tension, (b) $0 \leqq x \leqq$ a, and (c) in shear $0 \leqq x \leqq$ b increases, where x is the distance from the end of the element. For the (b) stage, there are two possible stages after further loading. If the fibre does not yield in shear, (d) "a" reaches $l/2$, but if (e) the fibre yields in shear before "a" reaches $l/2$, the fibre shows yielding in shear. For stage (c), there is only one possible stage after further loading; namely the region of shear plastic deformation of the fibre grows and the region of tensile plastic deformation appears (f). (As the stress distribution is symmetrical with the centre $x = l/2$, the shear stress between 1 and 2 at $x = l/2$ is always zero. Therefore the range of shear plastic deformation cannot grow beyond $x = l/2$. This is the reason why there are no stages other than (f) after stage (c).) After the appearance of stage (f), the region

TABLE I Regions contained in the deformation stages (a) to (g) shown in Fig. 3. The A to D refer to the regions A to D, respectively

Stage in Fig. 3	Regions and their ranges
(a)	A($0 \leqq x \leqq l/2$)
(b)	B($0 \leqq x \leqq a$) and A($a \leqq x \leqq l/2$)
(c)	C($0 \leqq x \leqq b$) and A($b \leqq x \leqq l/2$)
(d)	B($0 \leqq x \leqq l/2$)
(e)	D($0 \leqq x \leqq c$), B($c \leqq x \leqq a$) and A($a \leqq x \leqq l/2$)
(f)	D($0 \leqq x \leqq c$), C($c \leqq x \leqq b$) and A ($b \leqq x \leqq l/2$)
(g)	D($0 \leqq x \leqq c$) and B($c \leqq x \leqq l/2$)

of tensile deformation grows and stage (e) appears. After further loading for stages (d) and (e), stage (g) will appear where the fibre shows tensile plastic deformation in the whole length l, and shear plastic deformation for $0 \leqq x \leqq c$ but shear elastic deformation for $c \leqq x \leqq l/2$.

Noting the region where the fibre deforms elastically both in tension and shear as region A, the region where fibre deforms plastically in tension but elastically in shear as region B, the region where the fibre deforms plastically in shear but elastically in tension as region C and the region where the fibre deforms plastically both in tension and shear as region D, the aforementioned deformation stages shown in Fig. 3 consists of one, two or three regions of these regions, as shown in Table I.

2.4. Equations of stress equilibrium

In order to calculate the stress distribution in stages (a) to (g), we should first formulate the stress equilibrium in regions A to D. In the present work, to obtain equations of stress equilibrium, we modify the Dow's model [12], which was originally proposed to estimate the stress transfer from the matrix to discontinuous fibres in elastic fibre–elastic matrix composites.

2.4.1. Region A where the fibre deforms elastically both in tension and shear.

Defining $\bar{r}_1$ and $\bar{r}_2$ as the distance of the centroid of the fibre from the interface and as that of coating film from the interface, respectively, $\bar{r}_1$ and $\bar{r}_2$ are given by

$$\bar{r}_1 = d/2 - (2)^{1/2}d/4 \quad (6)$$

$$\bar{r}_2 = \{[(d + 2c)^2 + d^2]/8\}^{1/2} - d/2 \quad (7)$$

Equations for shear stress at interface, τ_i, are given by

$$\tau_i = -G_1(U_i - U_1)/\bar{r}_1 \quad (8)$$

$$\tau_i = -G_2(U_2 - U_i)/\bar{r}_2 \quad (9)$$

where U_1, U_2 and U_i are displacements of the fibre at the centroid, that of coating film at the centroid and that of the interface in the x direction. Combining Equations 8 and 9, we have

$$\tau_i = -H(U_2 - U_1) \quad (10)$$

$$H = [(G_1G_2/\bar{r}_1\bar{r}_2)]/[(G_1/\bar{r}_1) + (G_2/\bar{r}_2)] \quad (11)$$

As the load in the fibre and that in the coating film vary through interface we have

$$\bar{A}_1E_1(d^2U_1^A/dx^2) = \pi d\tau_i = -\pi dH(U_2^A - U_1^A) \quad (12)$$

$$\bar{A}_2E_2(d^2U_2^A/dx^2) = -\pi d\tau_i = \pi dH(U_2^A - U_1^A) \quad (13)$$

where $\bar{A}_1$ and $\bar{A}_2$ are cross-sectional areas of the fibre and the coating film, respectively. Solving Equations 12 and 13, we have

$$U_1^A = -(\mu A_1/k^2)\exp(-kx) - (\mu A_2/k^2)\exp(kx) + A_3x + A_4 \quad (14)$$

$$U_2^A = (A_1/k^2)\exp(-kx) + (A_2/k^2)\exp(kx) + A_3x + A_4 \quad (15)$$

where A_1 to A_4 are integral constants, μ is given by

$$\mu = \bar{A}_2E_2/\bar{A}_1E_1 \quad (16)$$

and k is given by

$$k = \{[\pi dH(1 + \mu)]/(\bar{A}_2E_2)\}^{1/2} \quad (17)$$

2.4.2. Region B where the fibre deforms plastically in tension but elastically in shear

The shear stress at the interface is given by Equations 10 and 11, similarly to region A. Using Equation 3, the equations for stress equilibrium are given by

$$\omega\bar{A}_1E_1(d^2U_1^B/dx^2) = -\pi dH(U_2^B - U_1^B) \quad (18)$$

$$\bar{A}_2E_2(d^2U_2^B/dx^2) = \pi dH(U_2^B - U_1^B) \quad (19)$$

Solving Equations 18 and 19, we have

$$U_1^B = -(\mu B_1/\omega r^2)\exp(-rx) - (\mu B_2/\omega r^2)\exp(rx) + B_3x + B_4 \quad (20)$$

$$U_2^B = (B_1/r^2)\exp(-rx) + (B_2/r^2)\exp(rx) + B_3x + B_4 \quad (21)$$

where B_1 to B_4 are integral constants and r is given by

$$r = \{[\pi dH(1 + \omega/\mu)]/(\bar{A}_2E_2)\}^{1/2} \quad (22)$$

2.4.3. Region C where the fibre deforms elastically in tension but plastically in shear

In this region, as the fibre is plastic in shear, using Equation 5, we have the interfacial shear stress as

$$\tau_i = -[(1 - \beta)\tau_{1y} + \beta G_1(U_i - U_1)/\bar{r}_1] \quad (23)$$

$$\tau_i = -G_2(U_2 - U_i)/\bar{r}_2 \quad (24)$$

Combining Equations 23 and 24, we have

$$\tau_i = \tau'_{1y} - J(U_2 - U_1) \quad (25)$$

$$\tau'_{1y} = [-(G_2/\bar{r}_2)(1 - \beta)\tau_{1y}]/[(\beta G_1/\bar{r}_1) + (G_2/\bar{r}_2)] \quad (26)$$

$$J = [(\beta G_1G_2/\bar{r}_1\bar{r}_2)]/[(\beta G_1/\bar{r}_1) + (G_2/\bar{r}_2)] \quad (27)$$

The equations for stress equilibrium are given by

$$\bar{A}_1E_1(d^2U_1^C/dx^2) = \pi d[\tau'_{1y} - J(U_2^C - U_1^C)] \quad (28)$$

$$\bar{A}_2E_2(d^2U_2^C/dx^2) = -\pi d[\tau'_{1y} - J(U_2^C - U_1^C)] \quad (29)$$

Solving Equations 28 and 29, we have

$$U_1^C = -(\mu C_1/t^2)\exp(-tx) - (\mu C_2/t^2)\exp(tx) + C_3x + C_4 \quad (30)$$

$$U_2^C = (C_1/t^2)\exp(-tx) + (C_2/t^2)\exp(tx) + C_3x + C_4 + \tau'_{1y}/J \quad (31)$$

where C_1 to C_4 are integral constants and t is given by

$$t = \{[\pi d(1 + \mu)J]/(\bar{A}_2E_2)\}^{1/2} \quad (32)$$

2.4.4. Region D where the fibre deforms plastically both in tension and shear

The interfacial stress is given by Equations 25 to 27. The equations for stress equilibrium are given by

$$\omega\bar{A}_1E_1(d^2U_1^D/dx^2) = \pi d[\tau'_{1y} - J(U_2^C - U_1^C)] \quad (33)$$

$$\bar{A}_2E_2(d^2U_2^D/dx^2) = -\pi d[\tau'_{1y} - J(U_2^C - U_1^C)] \quad (34)$$

Solving Equations 33 and 34, we have

$$U_1^D = -(\mu D_1/\omega s^2)\exp(-sx) - (\mu D_2/\omega s^2)\exp(sx) + D_3x + D_4 \quad (35)$$

$$U_2^D = (D_1/s^2)\exp(-sx) + (D_2/s^2)\exp(sx) + D_3x + D_4 + \tau'_{1y}/J \quad (36)$$

where D_1 to D_4 are integral constants and s is given by

$$s = \{[\pi dJ(1 + \mu/\omega)]/(\bar{A}_2E_2)\}^{1/2} \quad (37)$$

2.5. Boundary conditions

As stated in section 2.3., there are many deformation stages. In each stage, there are one to three regions as shown in Table I. The principle boundary conditions in each deformation stage are given as follows.

(a) At $x = 0$, the displacement of the fibre is zero, and the stress of the coating film is zero since it is fractured at $x = 0$ in the definition.

(b) At $x = x$ (including a, b and c), the displacement and tensile strain in fibre and coating film are continuous.

(c) At $x = a$ and b, the fibre shows yielding in tension and in shear, respectively. Therefore at $x = a$ and b, Equations 38 and 39 are satisfied, respectively.

$$E_1(dU_1(a)/dx) = \sigma_{1y} \quad (38)$$

$$H[U_2(b) - U_1(b)] = \tau_{1y} \quad (39)$$

At $x = c$, the fibre shows yielding both in tension and in shear. There are three possible cases for region D to arise; (e), (f) and (g) in Fig. 3. In the cases of (e) and (g), as the fibre is yielded in tension beyond $x = c$, the condition at $x = c$ gives

$$H[U_2(c) - U_1(c)] = \tau_{1y} \quad (40)$$

On the other hand, in the case of (f), as the fibre is yielded in shear beyond $x = c$, the condition at $x = c$ gives

$$E_1(dU_1(c)/dx) = \sigma_{1y} \quad (41)$$

(d) As the deformation behaviour of the element is symmetric with the centre at $x = l/2$, the displacement of the fibre and the coating film are equal to each other at $x = l/2$.

(e) At any cross-section, the load is constant, being equal to $\sigma_c(\bar{A}_1 + \bar{A}_2)$ where σ_c is the tensile stress of composite based on the total cross-sectional area.

Using above principle, the boundary conditions in each deformation stage are given as shown in Table II.

In the following calculation, the relation of β to ω was given to a first approximation as follows. As the relation of σ_1 to τ_1 and that of ε to γ in the plastic state are generally given by

$$\sigma_1 = M\tau_1 \quad (42)$$

TABLE II Boundary conditions in deformation stages (a) to (g) shown in Fig. 3

Stage in Fig. 3	Boundary conditions
(a)	$U_1^A(0) = 0$ . . . (1), $dU_2^A(0)/dx = 0$ . . . (2), $U_1^A(l/2) = U_2^A(l/2)$ . . . (3), $\bar{A}_1E_1[dU_1^A(x)/dx] + \bar{A}_2E_2[dU_2^A(x)/dx] = \sigma_c(\bar{A}_1 + \bar{A}_2)$ . . . (4)
(b)	$U_1^B(0) = 0$ . . . (1), $dU_2^B(0)/dx = 0$ . . . (2), $U_1^B(a) = U_1^A(a)$ . . . (3), $U_2^B(a) = U_2^A(a)$ . . . (4), $dU_1^B(a)/dx = dU_1^A(a)/dx$ . . . (5), $dU_2^B(a)/dx = dU_2^A(a)/dx$ . . . (6), $E_1[dU_1^A(a)/dx] = \sigma_{1y}$ . . . (7), $U_1^A(l/2) = U_2^A(l/2)$ . . . (8), $\bar{A}_1E_1\{dU_1^A(x)/dx\} + \bar{A}_2E_2\{dU_2^A(x)/dx\} = \sigma_c(\bar{A}_1 + \bar{A}_2)$ . . . (9)
(c)	$U_1^C(0) = 0$ . . . (1), $dU_2^C(0)/dx = 0$ . . . (2), $U_1^C(b) = U_1^A(b)$ . . . (3), $U_2^C(b) = U_2^A(b)$ . . . (4), $dU_1^C(b)/dx = dU_1^A(b)/dx$ . . . (5), $dU_2^C(b)/dx = dU_2^A(b)/dx$ . . . (6) $H[U_2^A(b) - U_1^A(c)] = \tau_{1y}$ . . . (7), $U_1^A(l/2) = U_2^A(l/2)$ . . . (8), $\bar{A}_1E_1[dU_1^A(x)/dx] + \bar{A}_2E_2[dU_2^A(x)/dx] = \sigma_c(\bar{A}_1 + \bar{A}_2)$ . . . (9)
(d)	$U_1^B(0) = 0$ . . . (1), $dU_2^B(0)/dx = 0$ . . . (2), $U_1^B(l/2) = U_2^B(l/2)$ . . . (3), $\bar{A}_1\{(1 - \omega)\sigma_{1y} + \omega E_1[dU_1^B(x)/dx]\} + \bar{A}_2E_2[dU_2^B(x)/dx] = \sigma_c(\bar{A}_1 + \bar{A}_2)$ . . . (4)
(e)	$U_1^D(0) = 0$ . . . (1), $dU_2^D(0)/dx = 0$ . . . (2), $U_1^D(c) = U_1^B(c)$ . . . (3), $U_2^D(c) = U_2^B(c)$ . . . (4), $dU_1^D(c)/dx = dU_1^B(c)/dx$ . . . (5), $dU_2^D(c)/dx = dU_2^B(c)/dx$ . . . (6), $H[U_2^B(c) - U_1^B(c)] = \tau_{1y}$ . . . (7), $U_1^B(a) = U_1^A(a)$ . . . (8), $U_2^B(a) = U_2^A(a)$ . . . (9), $dU_1^B(a)/dx = dU_1^A(a)/dx$ . . . (10), $dU_2^B(a)/dx = dU_2^A(a)/dx$ . . . (11), $E_1[dU_1^A(a)/dx] = \sigma_{1y}$ . . . (12), $U_1^A(l/2) = U_2^A(l/2)$ . . . (13), $\bar{A}_1E_1[dU_1^A(x)/dx] + \bar{A}_2E_2[dU_2^A(x)/dx] = \sigma_c(\bar{A}_1 + \bar{A}_2)$ . . . (14)
(f)	$U_1^D(0) = 0$ . . . (1), $dU_2^D(0)/dx = 0$ . . . (2), $U_1^D(c) = U_1^C(c)$ . . . (3), $U_2^D(c) = U_2^C(c)$ . . . (4), $dU_1^D(c)/dx = dU_1^C(c)/dx$ . . . (5), $dU_2^D(c)/dx = dU_2^C(c)/dx$ . . . (6), $E_1[dU_1^C(c)/dx] = \sigma_{1y}$ . . . (7), $U_1^C(b) = U_1^A(b)$ . . . (8), $U_2^C(b) = U_2^A(b)$ . . . (9), $dU_1^C(b)/dx = dU_1^A(b)/dx$ . . . (10), $dU_2^C(b)/dx = dU_2^A(b)/dx$ . . . (11), $H[U_2^A(b) - U_1^A(c)] = \tau_{1y}$ . . . (12), $U_1^A(l/2) = U_2^A(l/2)$ . . . (13), $\bar{A}_1E_1[dU_1^A(x)/dx] + \bar{A}_2E_2[dU_2^A(x)/dx] = \sigma_c(\bar{A}_1 + \bar{A}_2)$ . . . (14)
(g)	$U_1^D(0) = 0$ . . . (1), $dU_2^D(0)/dx = 0$ . . . (2), $U_1^D(c) = U_1^B(c)$ . . . (3), $U_2^D(c) = U_2^B(c)$ . . . (4), $dU_1^D(c)/dx = dU_1^B(c)/dx$ . . . (5), $dU_2^D(c)/dx = dU_2^B(c)/dx$ . . . (6), $H[U_2^B(c) - U_1^B(c)] = \tau_{1y}$ . . . (7), $U_1^B(l/2) = U_2^B(l/2)$ . . . (8) $\bar{A}_1\{(1 - \omega)\sigma_{1y} + \omega E_1[dU_1^B(x)/dx]\} + \bar{A}_2E_2[dU_2^B(x)/dx] = \sigma_c(\bar{A}_1 + \bar{A}_2)$ . . . (9)

$$\varepsilon = M\gamma \tag{43}$$

where M is a constant. When the material 1 is composed of a single crystal, M is given by the Schmidt factor, and when it is composed of a polycrystal, M is normally given by 2 or the Taylor factor (3.06 for f c c and 2.75 for b c c metals). From Equations 3 and 5, we have

$$d\sigma_1/d\varepsilon = \omega E \tag{44}$$

$$d\tau_1/d\gamma = \beta G_1 \tag{45}$$

Combining Equations 42 to 45, we have

$$\beta = \omega E_1/(M^2 G_1) \tag{46}$$

In the present calculations, the value of $M = 2$ was used since the metal fibre is generally composed of a polycrystal. Even if the Taylor factor were used, the results of the present calculation would not be changed essentially.

3. Results of the calculations

3.1. Tensile stress distribution in the segmented coating film and shear stress distribution at the interface as a function of the distance from the end of the segments

The tensile stress distribution in the segmented coating film σ_2 and the shear stress distribution at the interface τ_i as a function of x for given lengths of $l = 50$ (a,a'), 100 (b,b') and 200 μm (c,c') of segments were calculated as examples as shown in Figs 4 and 5 where the values of $E_1 = 100$ GPa, $E_2 = 300$ GPa, $G_1 = 40$ GPa, $G_2 = 120$ GPa, $d = 300\,\mu$m, $\omega = 0.005$, $\beta = 0.00313$, $\sigma_{1y} = 300$ MPa, $\tau_{1y} = 150$ MPa, and $c = 3\,\mu$m (a to c) and $10\,\mu$m (a' to c') were substituted. In these examples, the curves 1 to 3 correspond to $\sigma_c = 200$, 360 and 420 MPa, respectively. τ_i is taken as positive for the $-x$ direction for convenience. "$\sigma_c = 200$ MPa" corresponds to stage (a) in Fig. 3 and "$\sigma_c = 360$ MPa" and "$\sigma_c = 420$ MPa" correspond to stage (g) in Fig. 3. The tensile stress of the segments, σ_2, increases with increasing composite stress σ_c at any x except $x = 0$ for any values of l and c. Comparing the curves in (a) to (c) with those in (a') to (c') in Fig. 4, respectively, it is found that the $\sigma_2 - x$ curves for smaller c are higher than those for larger c. This implies that the thinner the coating film, the higher becomes the exerted tensile stress on the coating film. From the comparison of the curves in (a,a') with those in (b,b') and those in (c,c') in Fig. 4, it is known that high tensile stress is exerted on the segments when the length of the segments is long. The maximum stress of the segments, which is found at $x = l/2$, $\sigma_{2,\max}$ in Fig. 4, decreases with decreasing l. This means that the long segments can be broken into shorter segments, since the longer the segments, the higher becomes the exerted tensile stress, and therefore the probability where the exerted stress is higher than the ultimate tensile strength of the segments becomes high.

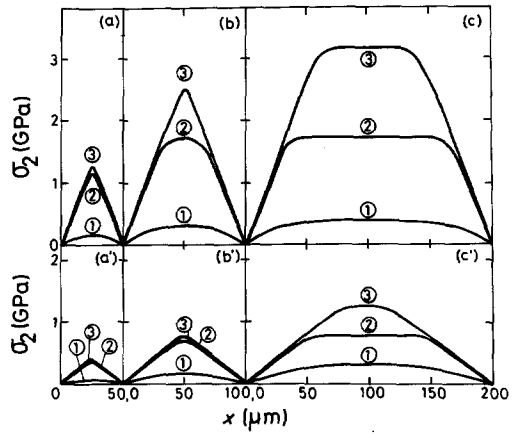

Figure 4 Tensile stress distribution in segments as a function of x for (a,a') $l = 50$, (b,b') 100 and (c,c') 200 μm at $\sigma_c = (①)$ 260, (②) 360 and (③) 420 MPa. (a) to (c) show the distributions for $c = 3\,\mu$m and (a') to (c') for $c = 10\,\mu$m. $E_1 = 100$ GPa, $E_2 = 300$ GPa, $G_1 = 40$ GPa, $G_2 = 120$ GPa, $d = 300\,\mu$m, $\omega = 0.005$, $\beta = 0.00313$, $\sigma_{1y} = 300$ MPa and $\tau_{1y} = 150$ MPa.

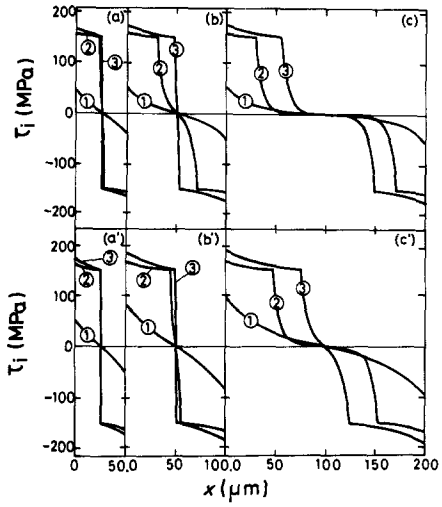

Figure 5 Shear stress distribution at the interface as a function of x for (a,a') $l = 50$, (b,b') 100 and (c,c') 200 μm at $\sigma_c = (①)$ 260, (②) 360 and (③) 420 MPa. (a) to (c) show the distributions for $c = 3\,\mu$m and (a') to (c') for $c = 10\,\mu$m. $E_1 = 100$ GPa, $E_2 = 300$ GPa, $G_1 = 40$ GPa, $G_2 = 120$ GPa, $d = 300\,\mu$m, $\omega = 0.005$, $\beta = 0.00313$, $\sigma_{1y} = 300$ MPa and $\tau_{1y} = 150$ MPa.

The shear stress distribution at the interface τ_i calculated using the same conditions as those in Fig. 4 is shown in Fig. 5 where (a) to (c) correspond to (a) to (c) in Fig. 4 and also (a') to (c') correspond to (a') to (c') in Fig. 4, respectively. The results in Fig. 5 show that (i) τ_i at $x = 0$ increases with increasing σ_c for any values of l and c, (ii) the length of the region where the fibre has been yielded in shear: namely the region where $\tau_i \geqq \tau_{1y}$ (150 MPa in this case), increases with increasing σ_c until this length approaches $l/2$, (iii) when l is short, the length of the region of $\tau_i \geqq \tau_{1y}$ approaches $l/2$ at low stress level and (iv) when the value of c is large, the length of the region of $\tau_i \geqq \tau_{1y}$ approaches $l/2$ at low stress level.

Figs 6 and 7 show σ_2–x and $\tau_i - x$ curves, respectively, for $l = 200\,\mu$m, $E_1 = 100$ GPa, $E_2 = 300$ GPa, $G_1 = 40$ GPa, $G_2 = 120$ GPa, $d = 1$ mm, $c = 10\,\mu$m, $\omega = 0.005$, $\beta = 0.00313$, and $\sigma_{1y} = 100$ MPa and $\tau_{1y} = 50$ MPa (curve 1), $\sigma_{1y} = 200$ MPa and $\tau_{1y} = 100$ MPa (2), and $\sigma_{1y} = 300$ MPa and $\tau_{1y} = 150$ MPa (3) at (a) $\sigma_c = 80$, (b) 200, (c) 320 and (d) 440 MPa. These examples show the effects of the yield

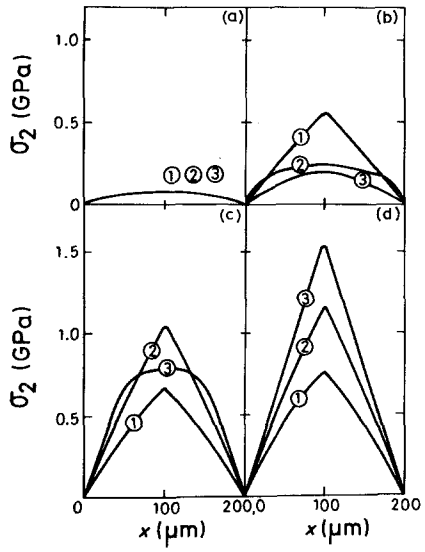

Figure 6 Tensile stress distribution in segments as a function of x for σ_{1y} = 100 (①), 200 (②) and 300 MPa (③) at σ_c = (a) 80, (b) 200, (c) 320 and (d) 440 MPa. E_1 = 100 GPa, E_2 = 300 GPa, G_1 = 40 GPa, G_2 = 120 GPa, ω = 0.005, β = 0.00313, d = 1 mm, l = 200 μm and c = 10 μm.

stress of fibre on the stress distributions. At σ_c = 80 MPa, the curves 1 to 3 correspond to stage (a) in Fig. 3, at σ_c = 200 MPa, the curves 1, 2 and 3 correspond to stages (g), (e) and (a), respectively, and at 320 and 440 MPa, they correspond to stage (g). Figs 6 and 7 show the following features.

1. At low stress level such as σ_c = 80 MPa, the curves 1 to 3 are the same to each other, since at this stress level, neither tensile nor shear yielding of the fibre occur.

2. For any values of σ_{1y}, the σ_2 and τ_i at any x (except x = 0 for σ_2) increases with increasing σ_c.

3. When the yield stress of the fibre is low, the fibre yields in tension and shear at low stress levels. This raises the value of σ_2 even at low stress levels. For instance, at σ_c = 200 MPa where, for σ_{1y} = 100 MPa, the fibre has been yielded in tension for $0 \leqq x \leqq l/2$ (i.e. in the whole region) and in shear for $0 \leqq x \leqq 99\,\mu$m, for σ_{1y} = 200 MPa, the fibre has been yielded in tension for $0 \leqq x \leqq 44\,\mu$m and in shear for $0 \leqq x \leqq 1\,\mu$m, and for σ_{1y} = 300 MPa, the fibre deforms elastically both in tension and shear in the whole range of x, the maximum value of σ_2 at $x = l/2$, $\sigma_{2,max}$, for σ_{1y} = 100 MPa (1) is higher than that for σ_{1y} = 200 MPa (2) and $\sigma_{2,max}$ for 200 MPa (2) is higher than that for σ_{1y} = 300 MPa (3).

4. When the yield stress of the fibre is high, the σ_2 is low at low stress levels but it becomes high at high stress levels after yielding. Especially when σ_c is very high such as 440 MPa shown in (d), the height of σ_2 is in the same sequence of the largeness of σ_{1y}.

5. After yielding of the fibre in shear, τ_i decreases relatively slowly with increasing x for $0 \leqq x \leqq b$ but then rapidly for $b \leqq x \leqq l/2$. b approaches $l/2$ at high stress levels for any values of σ_{1y}.

6. τ_i at high stress level such as 440 MPa becomes high and the height of τ_i for high σ_{1y} is higher than that for low σ_{1y}. This difference in the height of τ_i results in the difference in tensile distribution in the segments as stated in 4, since the higher the value of τ_i, the more stress transfer can occur from the fibre to the segments.

3.2. Maximum shear stress at the interface as a function of the stress of the composites

The shear stress τ_i at the interface is highest at x = 0 and l) as already shown in Figs 5 and 7. Figs 8 and 9 show the variation of τ_i (x = 0) as a function of σ_c, where the values of E_1 = 100 GPa, E_2 = 300 GPa, G_1 = 40 GPa, G_2 = 120 GPa, ω = 0.005 and γ = 0.00313, and for Fig. 8 the values of d = 1 mm, c = 10 μm, σ_{1y} = 100 MPa (a) and 300 MPa (b) and l = 25, 50, 100 and 200 μm, and for Fig. 9 the values

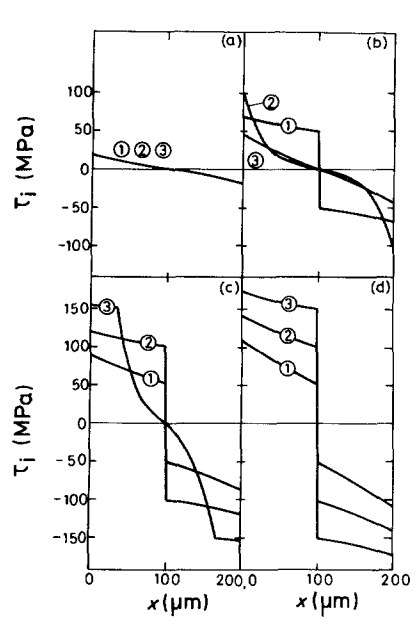

Figure 7 Shear stress distribution at the interface as a function of x for σ_{1y} = 100 (①), 200 (②) and 300 MPa (③) at σ_c = (a) 80, (b) 200, (c) 320 and (d) 440 MPa. E_1 = 100 GPa, E_2 = 300 GPa, G_1 = 40 GPa, G_2 = 120 GPa, ω = 0.005, β = 0.00313, d = 1 mm, l = 200 μm and c = 10 μm.

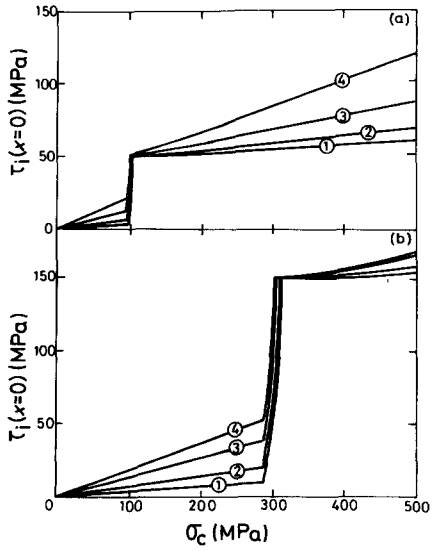

Figure 8 Variation of τ_i (x = 0) as a function of σ_c for σ_{1y} = (a) 100 and (b) 300 MPa for l = 25 (①), 50 (②), 100 (③) and 200 m (④). E_1 = 100 GPa, E_2 = 300 GPa, G_1 = 40 GPa, G_2 = 120 GPa, ω = 0.005, β = 0.00313, d = 1 mm and c = 10 μm.

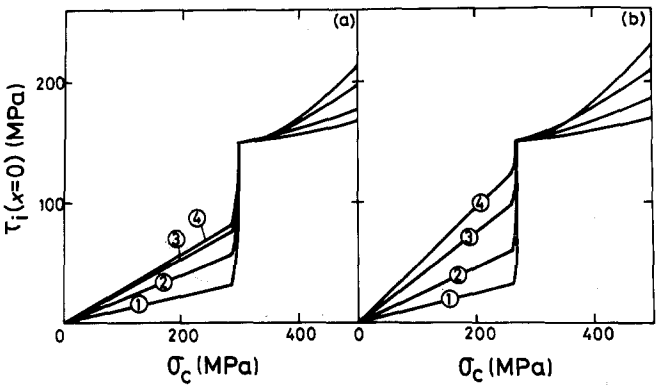

Figure 9 Variation of τ_i ($x = 0$) as a function of σ_c for (a) $c = 3\,\mu m$ and (b) $10\,\mu m$ for $l = 25$ (①), 50 (②), 100 (③) and $200\,\mu m$ (④). $E_1 = 100\,GPa$, $E_2 = 300\,GPa$, $G_1 = 40\,GPa$, $G_2 = 120\,GPa$, $\omega = 0.005$, $\beta = 0.00313$, $\sigma_y = 300\,MPa$ and $d = 300\,\mu m$.

of $d = 300\,\mu m$, $c = 3\,\mu m$ (a) and $10\,\mu m$ (b), $\sigma_{1y} = 300\,MPa$, and $l = 25$, 50, 100 and $200\,\mu m$, were used in the calculation. The following features are shown in Figs 8 and 9.

(i) The longer is l, the higher is τ_i ($x = 0$).

(ii) The larger is c, the higher is τ_i ($x = 0$).

(iii) τ_i ($x = 0$) increases linearly with increasing σ_c in the initial portion but then very rapidly in the second portion and gradually in the final portion. The initial linear portion corresponds to stage (a), the second portion to (b) and (d) or (e), and the final portion to (g) in Fig. 3. Taking the examples shown in Fig. 8a and b, the curves 1 to 3 experience the stages (a) → (b) → (d) → (g) and the curve 4 the stages (a) → (b) → (e) → (g). In all examples investigated, the range of the second portion consisting of the stages (b) and (d) or (e) was very narrow. This result could be explained as follows. When tensile yielding of the fibre at $x = 0$ occurs and stage (b) arises, the deformation amount (strain) of the fibre at $x = 0$ should be more than that in stage (a) to support the applied load. This increment in deformation amount in the fibre causes large differences in deformation between the fibre and the segments, which rapidly raises the interfacial stress. In this way, the interfacial stress at $x = 0$ becomes τ_{1y} after a small load increment and stage (g) arises. In stage (g), τ_i ($x = 0$) increases gradually since the shear strain hardening coefficient is normally low ($\beta = 0.00313$ in this calculation).

3.3. Maximum exerted tensile stress in segments as a function of stress of composites

As shown in Figs 4 and 6, the segments are pulled in tension and the maximum exerted tensile stress in the segments is found at $x = l/2$. The maximum tensile stress in segments $\sigma_{2,max}$ becomes high with increasing σ_c. The variation of $\sigma_{2,max}$ as a function of σ_c is influenced by the geometrical factors such as d, l and c, and also by the mechanical factors such as E_1, E_2, G_1, G_2, σ_{1y}, τ_{1y} and so on. In this section, some examples showing the effects of these factors on $\sigma_{2,max}$–σ_c curves will be presented.

Figs 10 and 11 show how the geometrical factors affect the $\sigma_{2,max}$–σ_c curve. In these calculations, the values of $E_1 = 100\,GPa$, $E_2 = 300\,GPa$, $G_1 = 40\,GPa$, $G_2 = 120\,GPa$, $\omega = 0.005$, $\gamma = 0.00313$, $\sigma_{1y} = 300\,MPa$ and $\tau_{1y} = 150\,MPa$ were used and the values of d, c and l were varied. Fig. 12 shows the effects of the magnitude of σ_{1y} in which the values concerned with mechanical properties other than σ_{1y} and τ_{1y} were the same as those used in the calculation for Figs 10 and 11, and the values of d and c were taken to be 1 mm and $10\,\mu m$, respectively. Fig. 13 shows the effects of the magnitude of E_2 and G_2 under fixed values of $E_1 = 100\,GPa$, $G_1 = 40\,GPa$, $\sigma_{1y} = 200\,MPa$, $\tau_{1y} = 100\,MPa$, $\omega = 0.005$, $\gamma = 0.00313$, $d = 1\,mm$, $c = 10\,\mu m$ and $l = 200\,\mu m$. In this case, G_2 was calculated using the relation

$$G_2 = E_2/[2(1 + \nu_2)] \tag{47}$$

where ν_2 is Poisson's ratio of the coated layer, which was taken to be 0.25 in this work. The effects of the geometrical and mechanical factors on the $\sigma_{2,max}$–σ_c curves shown in Figs 10 to 13 are summarized as follows.

(i) In any case, $\sigma_{2,max}$ increases with increasing σ_c.

(ii) In the initial portion corresponding to stage (a) in Fig. 3, $\sigma_{2,max}$ increases linearly with increasing σ_c and in the second portion corresponding to stages (b) and (d) or (e), it increases rapidly. In the final portion corresponding to stage (g), the $\sigma_{2,max}$ for large l increases more than that for small l.

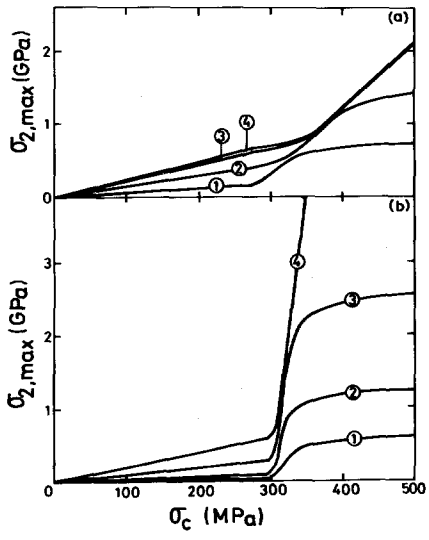

Figure 10 Variation of $\sigma_{2,max}$ as a function of σ_c for (a) $d = 100\,\mu m$ and (b) $d = 1\,mm$ for $l = 25$ (①), 50 (②), 100 (③) and $200\,\mu m$ (④). $E_1 = 100\,GPa$, $E_2 = 300\,GPa$, $G_1 = 40\,GPa$, $G_2 = 120\,GPa$, $\omega = 0.005$, $\gamma = 0.00313$, $\sigma_{1y} = 300\,MPa$ $\tau_{1y} = 150\,MPa$ and $c = 3\,\mu m$.

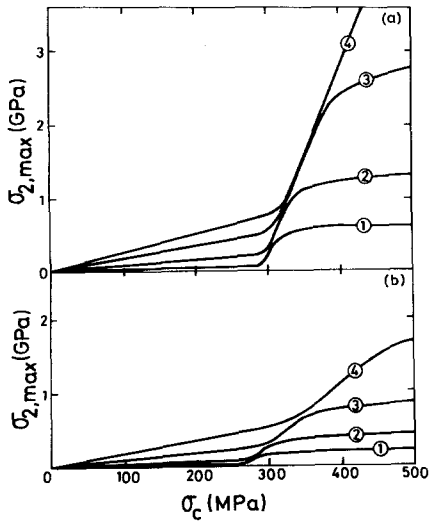

Figure 11 Variation of $\sigma_{2,max}$ as a function of σ_c for (a) $c = 3\,\mu m$ and (b) $c = 10\,\mu m$, for $l = 25$ (①), 50 (②), 100 (③) and 200 μm (④). $E_1 = 100\,GPa$, $E_2 = 300\,GPa$, $G_1 = 40\,GPa$, $G_2 = 120\,GPa$, $\omega = 0.005$, $\beta = 0.00313$, $\sigma_{1y} = 300\,MPa$, $\tau_{1y} = 150\,MPa$ and $d = 300\,\mu m$.

(iii) The longer the l, the higher the $\sigma_{2,max}$ at any stress level of σ_c.

(iv) The thicker the c for a given value of d, the lower the $\sigma_{2,max}$ at any stress level of σ_c.

(v) The larger the d for a given value of c, the higher the $\sigma_{2,max}$ at any stress level of σ_c.

(vi) As the second portion for low σ_{1y} arises at low stress levels of σ_c, $\sigma_{2,max}$ for low σ_{1y} is higher than that for high σ_{1y} since the stages (b) and (d) (or (e)), which raise τ_i as stated in Section 3.2, occur at low stress levels of σ_c for low σ_{1y}, while they do not occur at the same stress levels for high σ_{1y} (they occur at higher stress levels for higher σ_{1y}). On the other hand, in the final portion, the $\sigma_{2,max}$ for large σ_{1y} is higher than that for low σ_{1y} since the τ_i after occurrence of stage (g) is high for high σ_{1y} but low for low σ_{1y} as stated in Section 3.2.

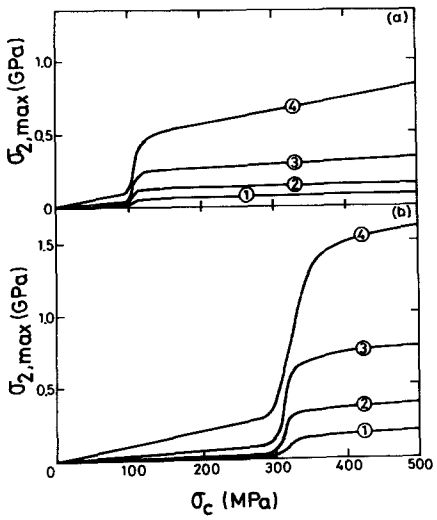

Figure 12 Variation of $\sigma_{2,max}$ as a function of σ_c for (a) $\sigma_{1y} = 100\,MPa$ and $\tau_{1y} = 50\,MPa$, and (b) $\sigma_{1y} = 300\,MPa$ and $\tau_{1y} = 150\,MPa$, for $l = 25$ (①), 50 (②), 100 (③) and 200 μm (④). $E_1 = 100\,GPa$, $E_2 = 300\,GPa$, $G_1 = 40\,GPa$, $G_2 = 120\,GPa$, $\omega = 0.005$, $\beta = 0.00313$, $d = 1\,mm$ and $c = 10\,\mu m$.

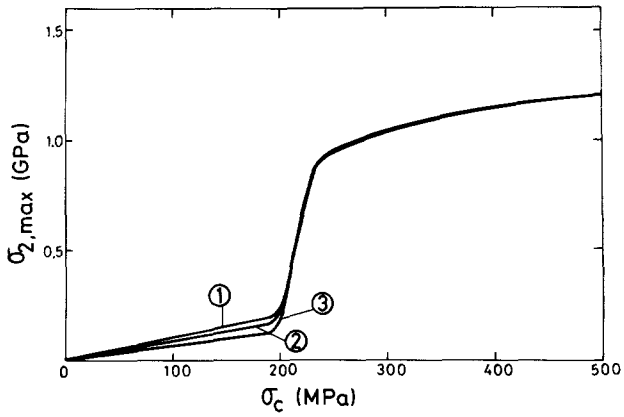

Figure 13 Variation of $\sigma_{2,max}$ as a function of σ_c for $E_2 = 300\,GPa$ and $G_2 = 120\,GPa$ (①), $E_2 = 200\,GPa$ and $G_2 = 80\,GPa$ (②), and $E_2 = 100\,GPa$ and $G_2 = 40\,GPa$ (③). $E_1 = 100\,GPa$, $G_1 = 40\,GPa$, $\omega = 0.005$, $\beta = 0.00313$, $\sigma_{1y} = 200\,MPa$, $\tau_{1y} = 100\,MPa$, $d = 1\,mm$, $c = 10\,\mu m$ and $l = 200\,\mu m$.

(vii) The higher the E_2 (and G_2), the higher the $\sigma_{2,max}$ in stage (a). However, in stage (g), the $\sigma_{2,max}$ for high E_2 is not so much different from that for low E_2.

In the present work, calculation was carried out for some combinations of the geometrical and mechanical factors. For other combinations, calculation can be carried out in a similar manner.

In the present approach, we have employed the shear lag analysis in order to estimate the stress transfer from fibre to broken segments, ignoring the radial and tangental stresses in the fibre and the segments. This gives a limit of application of the present approach to practical specimens. However, as the multiple-fracture of coating film occurs mainly by the increase of exerted stress on once-fractured coating film with increasing stress level, the stress transfer from the fibre segments is the most important process in multiple-fracture phenomenon. In this point, the present calculation method may be a useful tool to understand this phenomenon.

4. Conclusions

When a brittle film is coated onto the surface of a metal fibre (wire or rod), the coating film shows multiple-fracture under loading. In order to describe tensile stress distribution in segmented coating film and shear stress distribution at the interface between the fibre and the segment, a new approximate calculation method was presented, assuming that the interfacial bonding strength is high enough to prevent debonding. Using the present calculation method, effects of the geometrical factors such as fibre diameter, thickness of the coated layer and the length of segment as well as those of mechanical factors such as Young's modulus, shear modulus and yield stress of fibre and coating film on the stress distributions were described quantitatively.

References

1. S. OCHIAI, S. URAKAWA, K. AMEYAMA and Y. MURAKAMI, *Metall. Trans.* **11A** (1980) 525.
2. S. OCHIAI and Y. MURAKAMI, *ibid.* **12A** (1981) 684.
3. *Idem, Z. Metallkunde* **72** (1981) 827.
4. J. S. THORNTON and A. D. THOMAS Jr, *Metall. Trans.* **3** (1972) 637.

5. S. OCHIAI and Y. MURAKAMI, *Met. Sci.* **10** (1976) 401.
6. I. PFEIFFER and E. SPRINGER, *Z. Metallkunde* **63** (1977) 667.
7. S. NOURBAKHSH, Y. S. HASCICEK, M. J. GORINGE and J. W. MARTIN, *J. Mater. Sci.* **17** (1982) 3204.
8. T. SHIKATA, H. SHINNO, M. FUKUTOMI, M. FUJITSUKA and M. OKADA, *ibid.* **18** (1983) 3092.
9. *Idem, ibid.* **18** (1983) 3099.
10. A. KELLY and W. R. TYSON, *J. Mech. Phys. Solids* **13** (1965) 329.
11. S. OCHIAI and K. OSAMURA, *J. Mater. Sci.* **21** (1986) 2735.
12. N. F. DOW, GEC Missile and Space Division, Report No. R63SSD61, quoted by G. S. Holister and C. Thomas "Fibre Reinforced Materials" (Elsevier, London, 1966) p. 23.

Received 20 August
and accepted 4 October 1985